

Point defects in hexagonal silicon

Lin Sun ¹, Mário R. G. Marques,² Miguel A. L. Marques ^{2,3,*} and Silvana Botti ^{1,3,†}¹*Institut für Festkörpertheorie und -optik, Friedrich-Schiller-Universität Jena, Max-Wien-Platz 1, 07743 Jena, Germany*²*Institut für Physik, Martin-Luther-Universität Halle-Wittenberg, 06120 Halle (Saale), Germany*³*European Theoretical Spectroscopy Facility*

(Received 11 July 2020; revised 1 March 2021; accepted 9 June 2021; published 28 June 2021)

The importance of hexagonal Lonsdaleite silicon-germanium has been growing lately due to its possible uses in optoelectronic devices. However, very little is known about defects in the hexagonal phases of group-IV semiconductors. We extend here an efficient constrained structure prediction algorithm designed for interface reconstructions to the study of point defect geometries. With this method we perform an exhaustive structure prediction study of the most energetically favorable intrinsic defects in Lonsdaleite silicon. We obtain among the lowest-energy structures the hexagonal counterparts of all known defects of cubic silicon, together with other often more complex geometries. Neutral vacancies, fourfold-coordinated, and Frenkel defects have comparable formation energies in both hexagonal and cubic phases, while some interstitial defects become considerably more stable in the hexagonal lattice. Furthermore, due to the reduced symmetry, formation energies can depend on the orientation of the defect with respect to the c axis. Finally, we calculate the density of states of the defective supercells to determine which defects lead to electronic states in the band gap, potentially affecting the performance of optoelectronic devices based on hexagonal group-IV crystals.

DOI: [10.1103/PhysRevMaterials.5.064605](https://doi.org/10.1103/PhysRevMaterials.5.064605)

I. INTRODUCTION

Most technologically relevant semiconductors crystallize in either a face-centered cubic or a hexagonal closed-packed lattice. These closely related atomic arrangements differ by the stacking of atomic planes: An ABC stacking leads to the cubic phase, while the $ABAB$ stacking results in a hexagonal symmetry. For an elemental semiconductor, the two phases are commonly labeled as “diamond” and “Lonsdaleite” structure, respectively, while for a binary the terminology “zincblende” and “wurtzite” is used. The latter structures are obviously obtained through the coloring of the two sublattices of the former structures.

The energy difference between cubic and hexagonal packing is often very small, so the preferred choice for a certain composition is rather subtle and hard to predict. This is understandable, as the nearest neighbors and next-nearest neighbors are the same in the ideal wurtzite and zincblende structures. For example, carbon, silicon, germanium, GaAs, etc. have a cubic structure [1,2], while ZnO, ZnS, CdS, and CdSe are known to crystallize in the hexagonal phase [2].

The ground-state crystal structure of silicon, the most common semiconductor, is the diamond phase. This is perhaps the most studied crystal in solid-state physics, and every imaginable experimental probe or theory has been applied to it. However, many other low-energy phases of silicon, respecting the tetrahedral arrangement of the atoms, are possible [3–7], and some have been experimentally synthesized [8–13].

In recent years, interest in the Lonsdaleite phase of silicon and germanium has been growing. In fact, several methods

have been reported for the growth of hexagonal silicon, such as the diamond anvil cell technique at high pressures [14], the deposition of microcrystallites during laser ablation of SiO₂ films [15], the vapor-liquid-solid method [10,16], and the crystal structure transfer method [9,11]. Moreover, the latter method was shown to lead to large and stable regions of the pure hexagonal phase [9].

The importance of the hexagonal phase stems from theoretical calculations that predicted a tunable direct band gap for Si_{1-x}Ge_x alloys [5–7,17,18], which can increase the efficiency of light emission for these semiconductors. This has been recently confirmed by Fadaly *et al.* [19] who demonstrated experimentally efficient light emission from direct band-gap hexagonal Ge and SiGe alloys. Furthermore, by controlling the composition of the hexagonal SiGe alloy, they succeeded in changing continuously the emission wavelength over a broad range, while preserving the direct band gap [19]. This seminal result opened the way for the use of group-IV materials in optoelectronic applications.

It is well known that technological applications of semiconductors are extremely sensitive to the presence of defects and can be seriously hindered, or sometimes even enabled, by them. The defects of cubic silicon have already been extensively studied both experimentally and theoretically. In fact, by now we have detailed knowledge of which point defects are likely to exist in cubic silicon, their electronic properties, and their influence on functioning optoelectronic devices [20]. However, that knowledge is still to a large extent lacking for its hexagonal counterpart.

It is therefore our objective to fill this gap and perform an extensive study of structure-property relations of point defects in Lonsdaleite silicon. Our approach relies on a constrained structure prediction algorithm that has recently been proposed

*miguel.marques@physik.uni-halle.de

†silvana.botti@uni-jena.de

by some of us [21]. We will be focusing on the defect geometries and formation energies at zero temperature, while deferring finite temperature properties to future studies. Supercells are built for the selected point defects, and simple local relaxations of the atomic positions are performed at fixed cell parameters. Such an approach is somehow unsatisfactory. In the best case, many defects that are energetically unfavored are unnecessarily included in the study; and in the worse case, relevant low-energy defects are not included. We propose, therefore, to identify *a priori* the most stable defect configurations using structure prediction. This preliminary step is particularly relevant when new materials are studied—as in this case, where the hexagonal symmetry implies that the number of possible point defects is considerably larger than for cubic silicon—but it can also lead to surprises for well-studied materials. For example, the fourfold coordinated defect (FFCD) of cubic silicon was neglected for a long time in defect studies, as it was not stable in force-fields calculations and was only found very late using density functional theory (DFT) [22].

II. METHODS

Global structural prediction calculations [23] have grown in prominence in the past decade due to their ability to predict the low-energy crystal structures based solely on the composition of the material. This is extremely valuable, especially in situations where experiments are difficult or even impossible (such as in high-pressure environments [24–27]). The basic prediction algorithms are geared toward yielding low-energy bulk phases; however, a judicious use of geometrical constraints can allow us to study other physical systems. In fact, extensions have been put forward to investigate surfaces [28], two-dimensional systems [29–32], grain boundaries [21,33–35], line defects [36], etc.

Our algorithm of choice for the global structural prediction is the minima-hopping method [37,38]. This algorithm has already been used with success to predict surfaces [39,40], two-dimensional systems [41], line defects [36], clusters [42], bulk phases under pressure [25], etc. Furthermore, as it is based on a sequence of geometry optimizations followed by short molecular dynamics steps, it is rather simple to generalize in order to impose geometrical constraints. Of course, any other structural prediction algorithm, be it genetic algorithms [43,44], particle-swarm methods [45,46], random search [47–50], etc., could also be used for our purpose.

Here we generalize the constrained minima hopping method [21] to predict geometries of point defects. Our procedure is the following: (i) We build a supercell of the parent compound large enough to include the defect plus a buffer region. For our case of Lonsdaleite silicon, the starting supercell is an orthorhombic cell containing 72 unit cells (of the primitive hexagonal lattice) with lattice vectors $a = 15.4$, $b = 20.0$, and $c = 19.1$ Å. It contains 288 atoms and is depicted in Fig. 1. (ii) We select the atoms within a slab (more precisely, three layers of atoms) in each Cartesian direction and fix them to their equilibrium coordinates. These are the atoms in gray in Fig. 1. For the purposes of the algorithm, this buffer region should be thick enough to represent the bulk of hexagonal silicon, while the volume inscribed (atoms in

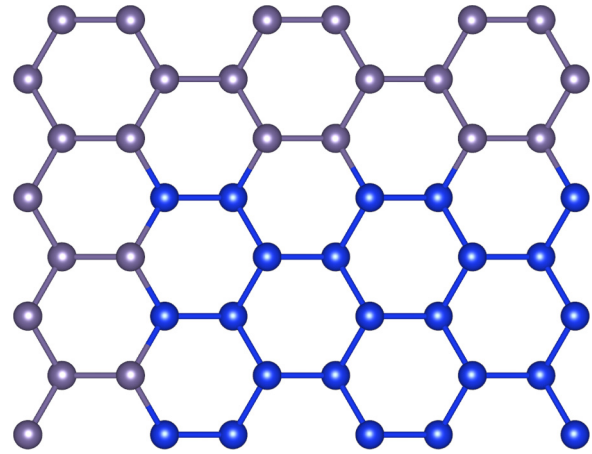


FIG. 1. Depiction of the (0001) surface of the constrained cell. In gray we show the silicon atoms that are fixed and in blue the atoms that are allowed to move. Note that there is a slab of silicon atoms in the perpendicular direction that are fixed, but that are not visible in the figure.

blue in the figure) should be large enough to contain the point defects. We also fix the lattice vectors. (iii) We may add or remove atoms from the blue region in case we want to study interstitials or vacancies. (iv) We perform global structural prediction simulations obeying the above constraints. This yields as the lowest possible structure the bulk phase (in this case hexagonal silicon), while metastable structures represent point defects.

Due to the geometrical constraints, it turns out that the same point defect located in different positions of the blue region will have slightly different energies as a consequence of the different strain imposed by the fixed atoms. As such, they will likely be misidentified by the global structural prediction algorithm as different defects. To resolve this issue, we perform an extra step in our methodology: (v) We eliminate the constraints on the atoms (while still keeping the lattice vectors fixed) and perform a reoptimization of the geometry.

The process of defect creation stems from the competition between the minimum internal energy of the ideal crystal and the stabilizing effect of entropy related to the disorder introduced by defect creation. Formally, the Gibbs' free energy of formation of a defect is given at temperature T and pressure P by the sum of the formation enthalpy and the entropic term $T \Delta S$. For single isolated defects, the variation of volume due to the creation of a point defect is negligible in the dilute case and the formation enthalpy can be approximated by the internal energy only. The entropic term can be split in the contributions of configurational entropy and phonons. It is well known that vibrational entropy of defects can give a sizable contribution to the free energy, but also configurational entropy can be non-negligible at temperatures near the melting point [51,52]. Including entropic terms is still challenging, especially within DFT, and we therefore limit our study to zero-temperature formation energies, which allows in any case for a fundamental first step in the understanding of defect thermodynamics.

The structural prediction algorithm requires an underlying theory that provides total energies and forces. This is often

DFT [53,54] as it assures unparalleled accuracy for a relatively modest computational effort. Unfortunately, structural prediction often requires tens or even hundreds of thousands of energy and force evaluations which, for a cell containing 288 atoms, is well beyond the computational capabilities of modern supercomputers. Therefore, we have to resort to more efficient (and inevitably less accurate) methods.

However, here we have to be careful. Despite the recognized usefulness of classical potentials to study structural properties of complex materials, and despite the existence of high quality potentials for silicon, deviations from DFT results have been demonstrated for calculations of silicon using classical potentials [55]. It is in particular known that force fields are not capable of stabilizing the lowest-energy point defect in silicon [22]. This is surprisingly true even for state-of-the-art machine-learning potentials [56]. A recent comparison with DFT results for a large dataset also shows that forces calculated with Stillinger-Weber or Tersoff force fields are consistently worse than forces calculated with DFT tight binding, provided that the tight-binding parameters are optimized to obtain at the same time energies and forces. [57]

In view of the above, we decided to use density-functional tight binding (DFTB), as implemented in DFTB+ [58]. This is a quantum mechanical approach, but that allows for much faster calculations than DFT. We used the parametrization from Ref. [59] that was specifically crafted for structural prediction runs, as the parameters are optimized to yield at the same time DFT-quality energies and forces. These same parameters gave excellent agreement with experiments for structural prediction of grain boundaries in silicon [21]. We remark that performing all calculations with DFT would require years in a supercomputer, while the DFTB calculations only took a few weeks with much more modest equipment. However, it is important to guarantee the reliability of the tight-binding method to prevent missing low-energy minima. We also verified that our methodology is able to obtain all lowest-energy defects of cubic silicon.

Finally, to eliminate the error introduced by the use of tight binding, we include a final step in our methodology: (vi) We perform a final geometry optimization of all interesting geometries using DFT. Our DFT calculations were performed with the Vienna Ab Initio Simulation Package (VASP) software [60,61] employing the projector augmented wave (PAW) method to model the core electrons. For the geometry optimizations and to calculate defect energies, we approximated the exchange-correlation functional with the Perdew-Burke-Ernzerhof (PBE) [62] approximation. In this case, we used an energy cutoff of 420 eV and a mesh of $1 \times 1 \times 1$ k-points for the geometry optimization and $4 \times 3 \times 3$ for the calculation of formation energies. This leads to a precision in the defect formation energies better than a hundredth of an eV. It is harder to estimate the intrinsic accuracy of DFT functionals in evaluating defect formation energies. In any case, we should remember that we are calculating energy differences of structures that are chemically similar, so we expect that many of the errors are likely to cancel out in this process. We remark that we do not include here any finite-size or band-edge correction, as our present aim is to predict the lowest-energy defects in hexagonal silicon, and this should be largely unaffected by these corrections.

For the analysis of the electronic structure, we employed the modified Becke-Johnson potential of Tran and Blaha [63,64]. It is by now known that this is the best functional to calculate band gaps of semiconductors and insulators [65]. It is, in fact, even slightly better on average than the screened hybrid of Heyd and Scuseria from 2006 [66] at only a fraction of the computational effort. Moreover, it was recently shown that it yields a very good description of the hexagonal phase of silicon and germanium [18,19,67]. The modified Becke-Johnson has been used in the past to calculate the electronic structure of defects, for example, in ZrO_2 [68], in the mixed borate-carbonate $\text{Pb}_7\text{O}(\text{OH})_3(\text{CO}_3)_3(\text{BO}_3)$ [69], or in Mg_2X ($\text{X} = \text{Si}, \text{Ge}, \text{Sn}$) [70]. The electronic density of states (DOS) calculations were performed using the tetrahedron method with a $2 \times 2 \times 2$ k-point grid.

Following this procedure, we performed a series of simulations for unit cells containing one or two vacancies (-1 or -2 atoms), one or two interstitials ($+1$ or $+2$ atoms), and with the pristine 288-atom cell. The atoms were added/removed to/from random positions in the lattice. For each case, we performed four independent minima-hopping runs, and each run was stopped after obtaining around 400 minima.

It is true that, in general, the charge state of the defect is essential to determine its thermodynamic and electronic properties. However, it was shown for cubic silicon that the vacancy is the only defect stabilized by charge, and this stabilization is rather small [71,72]. In view of that, in this work we concentrate on neutral defects only.

III. RESULTS AND DISCUSSION

A summary of the lowest-energy point defects stemming from our simulations of hexagonal silicon can be found in Table I, while in Fig. 2 we show the geometries of the defects. The crystallographic information files for all defects with energies ranging from 2.52 to 7.00 eV and a depiction of their geometries can be found in the Supplemental Material [75].

From the analysis of the runs, we found out that our structural prediction runs were able to identify the hexagonal counterparts of all common defects already known for cubic silicon. Furthermore, as the hexagonal lattice contains fewer equivalent sites than the cubic lattice, we found a series of variants of these defects. Note that a similar symmetry breaking has also been observed in some polymorphs of SiC [76,77].

To make the analysis clearer, we grouped defects with similar spacial arrangements and reported their energy range in Table I. The geometries of several low-energy variants can be found in the Supplemental Material [75]. In general, these variant defects can have quite different energies depending on their orientation. For example, we found two split (X) interstitials, oriented along different crystallographic directions, that possess quite different formation energies (2.54 and 3.27 eV). Another interesting example is the FFCD that possesses an energy ranging from 2.52 to 3.44 eV, depending on its orientation with respect to the hexagonal c axis. This anisotropic behavior, and the large energy differences between different defect orientations, suggests the possibility to observe in the experimental samples defect alignment along certain crystallographic directions.

TABLE I. PBE formation energy (in eV) of the lowest-energy point defects in hexagonal Si, compared (when possible) with the equivalent defect in cubic silicon. The square brackets in the column of hexagonal Si energies denote energy intervals for the possible orientations of each defect. Note that in the hexagonal lattice we obviously cannot have a tetrahedral interstitial due to symmetry, but there is a interstitial with a similar geometry, so we decided to keep the nomenclature.

Defect	Hexagonal Si Energy (eV)	Cubic Si Energy (eV)
Fourfold coordinated defect (FFCD)	[2.52, 2.65]	2.42 [22]
Tetrahedral (T) interstitial	[2.52, 2.60]	4.09 [73], 3.96 [74]
Split (X) interstitial	[2.54, 3.27]	3.31 [22], 3.67 [73], 3.66 [74]
Hexagonal (H) interstitial	[2.73, 3.25]	3.31 [22], 3.77 [73], 3.69 [74]
Extended split (EX) interstitial	[3.40, 4.63]	
FFCD2	[3.43, 3.44]	
Pentagonal (P) interstitial	[3.52, 4.97]	
EX2 interstitial	[3.82, 4.53]	
EX3 interstitial	[3.82, 4.68]	
Vacancy (V)	3.78	3.17 [22]
EX4 interstitial	[3.94, 4.99]	
Double (XT) interstitial	[4.11, 4.35]	
Frenkel	4.26	4.32 [22]
Di-vacancy	[5.48, 6.50]	

Of course, our simulations also yielded a plethora of more complex defects, some of them with energies in the same range as the most common defects. The lowest of these are

also listed in Table I, while some more can be found in the Supplemental Material [75].

In Table I we also compare the energy of the well-known point defects of the cubic (diamond) Si lattice [22] with their

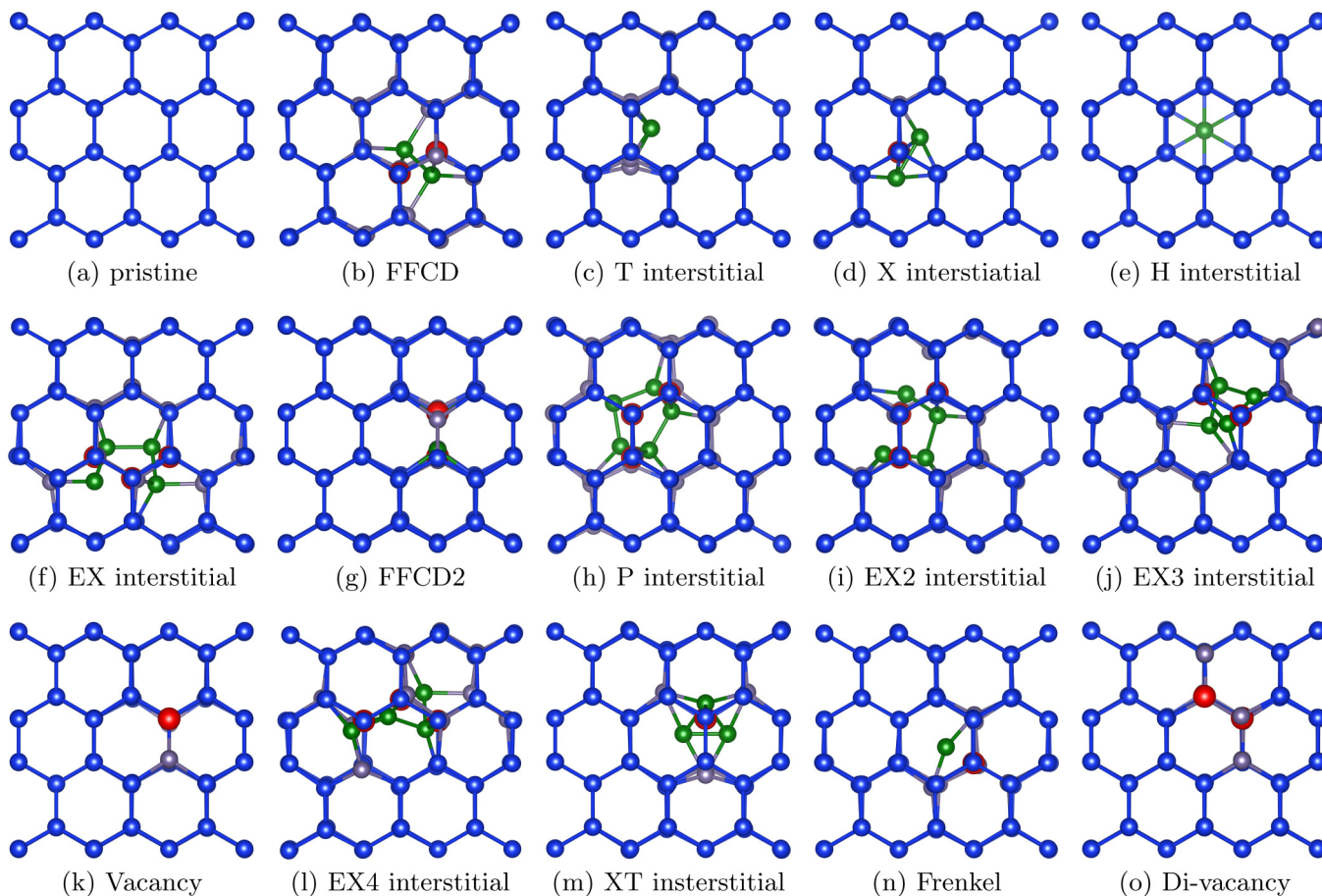


FIG. 2. Geometries of the lowest-energy defects of hexagonal silicon that stemmed from our simulations. Vacancies are depicted in red, interstitial atoms are in green, while atoms that are slightly displaced from their bulk positions are in gray.

hexagonal counterparts. We find that corresponding defects have to a large extent similar formation energies. This is consistent with the observation that Si has the same coordination in the considered cubic and hexagonal lattices. Perhaps not surprisingly, the energy to create a single vacancy [see Fig. 2(k)] in hexagonal silicon is essentially the same as for the cubic lattice. We also find that removing two neighboring silicon atoms [see Fig. 2(o)] is substantially more convenient (by around 2 eV) than creating two isolated vacancies.

The situation is more varied for interstitials, as their energy can be significantly lower in the hexagonal phase for certain defect orientations as a consequence of the lowered symmetry. This is true for the tetrahedral (T), split (X), hexagonal (H), and extended split (EX) interstitials, with the difference in energy between cubic and hexagonal silicon around 1 eV. These defects are expected therefore to be much more common in samples of hexagonal silicon.

The lowest-energy point defect of hexagonal silicon, as in cubic silicon [22], is the FFCD [see Fig. 2(b)]. This defect results from the rotation of two atoms, allowing to preserve the bond lengths and angles with respect to their bulk values, leading to a rather stable configuration. In particular, we observed that when the interstitials are aligned along the $[1\bar{1}20]$ direction they possess lower energy than when aligned along the $[1\bar{1}\bar{2}1]$ direction [see the FFCD2 defect depicted in Fig. 2(g)].

In terms of formation energy, the second lowest-energy defect is the tetrahedral interstitial [see Fig. 2(c)]. We note that, strictly speaking, this defect does not exhibit tetrahedral symmetry, as this is incompatible with the symmetry of the hexagonal lattice. We decided nevertheless to keep the nomenclature to simplify the discussion. The formation of this defect in this lattice requires the displacement of some of its surrounding atoms. The formation energy of this defect in the hexagonal lattice is ≈ 1 eV lower than in the cubic lattice, meaning that this defect becomes as stable as the FFCD.

The X interstitial appears afterward [see Fig. 2(d)]. In the diamond lattice, this defect is usually described as a dumbbell configuration formed by two silicon atoms oriented along the $[110]$ direction [78]. Moreover, a vacancy is located between these interstitials. In the hexagonal lattice, the silicon atoms can orient along the $[1\bar{1}20]$ or the $[1\bar{1}\bar{2}1]$ lattice direction, where the former configuration is more stable.

The H interstitial follows in terms of energy [see Fig. 2(e)]. In this defect, the interstitial atom is located at the center of the characteristic hexagons formed by the silicon atoms. The H interstitial is considerably important in Lonsdaleite, since its formation energy can be rather small. In fact, we found it to vary from 2.73 eV, when located at the center of an irregular hexagon, to 3.25 eV, when located at the center of the regular hexagons seen in the c direction. Note that this latter value is close to the energy of this defect in the cubic lattice.

Next comes the EX interstitial [see Fig. 2(f)]. Similarly to the X interstitial, this defect is also a dumbbell configuration. However, two additional atoms leave their pristine position and form a relatively symmetric “U”-shaped motif with the dumbbell interstitials. In total, three Si-sites are vacant. In the Lonsdaleite the dumbbell interstitials are also oriented along the $[1\bar{1}20]$ direction. We note that the shape of the

“U” can change due to the symmetry of the hexagonal lattice. Furthermore, we found several configurations where the atoms did not manage to form this U shape. Instead, they can fold to form a squared shape [see Fig. 2(j)] or even an L shape [see Fig. 2(l)]. In terms of energy, the U-shaped configurations have the lowest energy, as low as 3.40 eV, while certain configurations of the squared and L shape achieve 3.82 and 3.94 eV, respectively. We also observed another higher energy configuration (4.51 eV or higher) resembling the EX, but where two vacancies form a line in the c direction and are closer to one of the dumbbell interstitials.

The simulations with the 288-atom cell also yielded defects that are similar to the X and EX interstitial, the difference being that they also possess one vacant site. In particular, the latter is quite stable [see Fig. 2(i)].

The Frenkel defect [Fig. 2(n)] occurs when an atom abandons its lattice position in favor of an interstitial position. In both types of lattice this defect has a characteristic energy of around 4.30 eV.

Additionally, we would like to mention a couple of complex defect configurations: One where the interstitials form a pentagonal structure, with four vacancies and an energy of 3.52 eV [see Fig. 2(h)]; the second can be seen either as an FFCD combined with three interstitials forming a triangle-shape or as an EX combined with an additional dumbbell interstitial. It has a formation energy of 3.82 eV. Finally, we also found several interesting defects with energies between 4 and 5 eV, including combinations of the aforementioned interstitials, such as the XT di-interstitial [see Fig. 2(m)], the hexagonal analogous of the modified triangle, W, and Z di-interstitials [79], and many other complex defects.

We note that the concentration of point defects depends on the free energy of formation that can be approximated as the sum of the internal energy at zero temperature and the vibrational free energy. For cubic silicon, the calculation of the phonon contribution was performed for the neutral vacancy, the hexagonal and split self-interstitials, and the FFCD defect in Ref. [80], as well as for the vacancy in Ref. [81]. At high temperatures, the vibrational free energy associated with a point defect in silicon is of the order of 1 eV. This stabilization term is especially large for the vacancy and it turns out to be similar for all studied interstitials. We expect a similar situation for the hexagonal system due to its bonding similarity to cubic silicon. Unfortunately, we have to keep in mind a recent critical study [82] that casts serious doubts on the convergence of calculations of the vibrational free energy.

In order to gain some insight into the change of electronic properties induced by the presence of these defects, we computed the DOS for the most interesting defect structures. These results are presented in Fig. 3, where we plot the DOS for selected defects in an energy window around the band gap, as this is the region of most interest for optoelectronics. In all plots, the contribution to the DOS from the bulk region is perfectly visible by comparing to the DOS of pristine hexagonal silicon, depicted as a green line. In most cases, the states associated with the defects are found in the energy region close to the band gap. Note that, for some interstitials, we also find localized states at the bottom of the valence band (not shown).

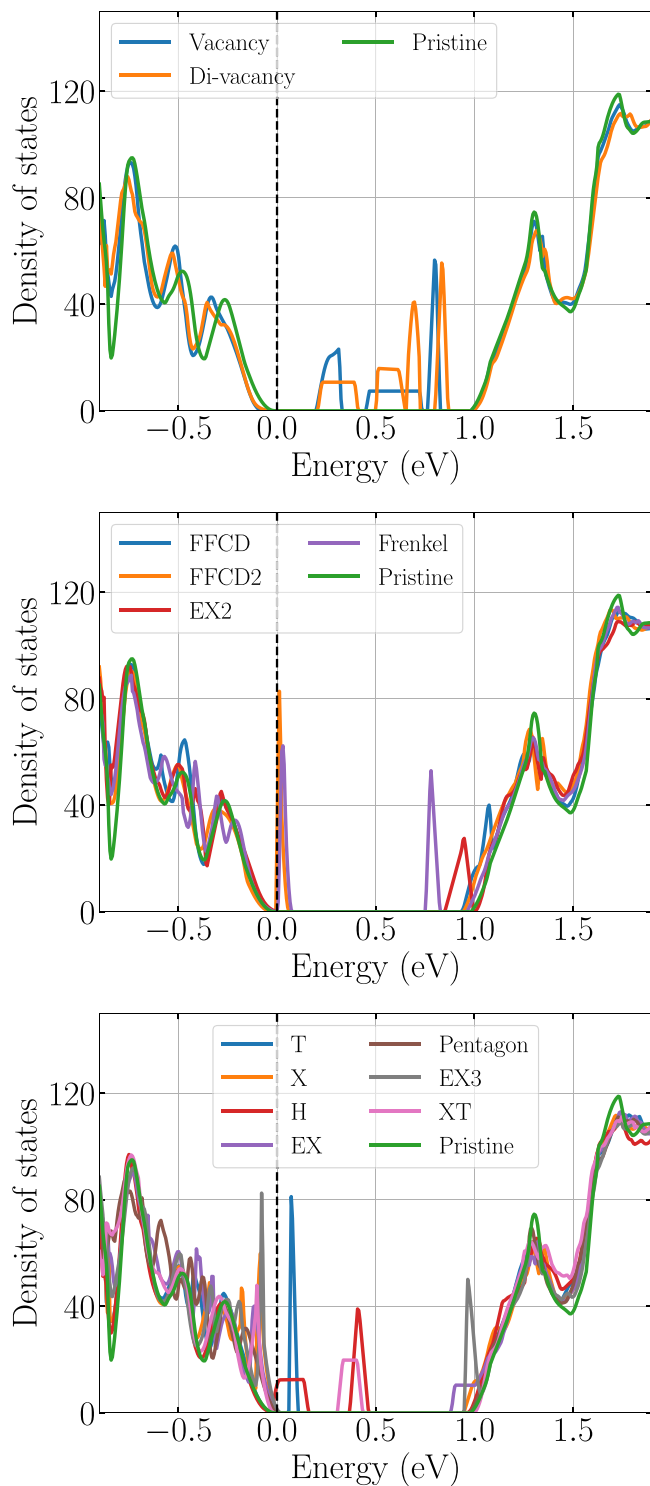


FIG. 3. Comparison between the DOS (around the band gap) of the pristine structure and the DOS of the structures containing defects: (Top panel) Vacancy and di-vacancy, (middle panel) defects conserving the number of atoms, (bottom panel) interstitial defects. All DOS were aligned to a characteristic peak in the valence band. For the pristine structure, this peak is located 3.1 eV below the Fermi level.

Both vacancies and di-vacancies can have a profound effect on the electrical properties of Lonsdaleite silicon. In fact, we find several deep states in the gap.

Turning our attention to defects that do not change the initial number of atoms of the 288-atom cell, we find that the FFCD does not lead to any defect states in the band gap, although we do find a localized state at the bottom of the conduction band. This situation is rather different when the interstitials align along the $[11\bar{2}1]$ direction (as in the FFCD2 structure), as we witness the appearance of a shallow state close to the top of the valence band. Finally, the Frenkel defect has a shallow state at the same position as the FFCD2 and also a localized state close to the bottom of the conduction band. In any case, the high formation energy of this defect is expected to limit its occurrence in experimental samples.

Finally, we analyze the modification to electronic band structure induced by the presence of interstitials. The lowest-energy defect of this kind, the T interstitial, exhibits a localized shallow state in the band gap close to the valence band edge. Both the X and the pentagonal interstitial do not induce electronic states in the band gap, but we can easily identify states coming from these defects in the valence band. The H and XT interstitials have deep states localized approximately in the middle of the band gap. Finally, the EX3 defect leads to defect states both at the top of the valence band and at the bottom of the conduction band. While the XT interstitial has a large formation energy and can be safely disregarded, optimized growth processes should be considered to reduce the occurrence of H interstitials.

IV. CONCLUSIONS

We performed a systematic investigation of the structure of lowest-energy point defects in the Lonsdaleite phase of silicon. To this end, we developed a constrained crystal structure prediction method to automatically search for point defects. The algorithm identified a plethora of low-energy point defects, including the analogous to all relevant defects known for diamond silicon.

Our method is fully unbiased and is capable of yielding the atomic configuration of low-energy defects, regardless of the chemistry or the crystal symmetry of the material. It can be particularly useful in the investigation of systems with either low symmetry or where defect complexes are expected to play an important role. Furthermore, and when coupled with a quantum-mechanical method to evaluate energies and forces, this approach can be trivially generalized to study charged defects.

A comparison of similar defects in the two hexagonal and cubic lattices reveals that some interstitial defects have lower energy in Lonsdaleite silicon, meaning that they will be more common in synthesized samples of hexagonal silicon than in diamond silicon. We note that in the Lonsdaleite phase, the fourfold-coordinated defect, the tetrahedral interstitial, and the split interstitial are the defects with the lowest formation energy (around 2.5 eV), while the vacancy is more than 0.5 eV higher than in cubic silicon. This latter difference is, in our opinion, very important for the emerging hexagonal silicon technology. At typical temperatures where silicon devices are thermally processed (around 1000–1100 K), both interstitials and vacancies seem to exist in roughly equal measure [80]. In fact, although the energy of the vacancy is considerably higher than the one for the interstitials, it is compensated by

a larger entropy contribution. Assuming a similar behavior of the entropy for the hexagonal case, we conclude that vacancies should be significantly less common in hexagonal silicon than in its cubic counterpart. Moreover, defects of the hexagonal silicon lattice admit several variants due to symmetry breaking and can have quite different energies depending on their relative orientation in the crystal lattice.

Analysis of the electronic DOS of the structures containing the defects reveals that the fourfold-coordinated defect is electronically benign, but that the tetrahedral and split interstitials exhibit localized shallow states slightly above and below the top of the valence band, respectively. Deep states in the gap were found for the vacancies and for the hexagonal and double interstitials.

As most experimental techniques do not allow to determine directly which point defects are present in a sample and, even less, their geometry, defect identification is usually

indirect, e.g., through some signatures that can be detected in spectroscopy experiments. Our first-principles study of the structure and associated DOS of the lowest-energy defects offer clear defect signatures that can be employed to interpret experiments of hexagonal silicon. Moreover, we propose our defect supercells as a reliable starting point for more comprehensive studies taking into account the contribution of finite temperatures.

ACKNOWLEDGMENTS

S.B. acknowledges financial support from the Deutsche Forschungsgemeinschaft (DFG, German Research Foundation) through the Collaborative Research Center CRC-1375 (Project A02) and the Project BO 4280/8-1 and from the European Union's Horizon 2020 research and innovation program under Grant Agreement No. 735008 (SiLAS).

-
- [1] M. L. Cohen and J. R. Chelikowsky, Diamond and Zinc-Blende structure semiconductors, in *Electronic Structure and Optical Properties of Semiconductors* (Springer, Berlin, Heidelberg, Germany, 1988), pp. 79–139.
- [2] F. H. Allen, G. Gergerhoff, and R. Sievers (eds.), *Crystallographic Databases* (International Union of Crystallography, Chester, England, 1987).
- [3] S. Botti, J. A. Flores-Livas, M. Amsler, S. Goedecker, and M. A. L. Marques, Low-energy silicon allotropes with strong absorption in the visible for photovoltaic applications, *Phys. Rev. B* **86**, 121204(R) (2012).
- [4] M. Amsler, S. Botti, M. A. L. Marques, T. J. Lenosky, and S. Goedecker, Low-density silicon allotropes for photovoltaic applications, *Phys. Rev. B* **92**, 014101 (2015).
- [5] J. D. Joannopoulos and M. L. Cohen, Electronic properties of complex crystalline and amorphous phases of Ge and Si. I. Density of states and band structures, *Phys. Rev. B* **7**, 2644 (1973).
- [6] J. D. Joannopoulos and M. L. Cohen, Electronic properties of complex crystalline and amorphous phases of Ge and Si. II. Band structure and optical properties, *Phys. Rev. B* **8**, 2733 (1973).
- [7] A. De and C. E. Pryor, Electronic structure and optical properties of Si, Ge and diamond in the lonsdaleite phase, *J. Phys. Condens. Matter* **26**, 045801 (2014).
- [8] D. Y. Kim, S. Stefanoski, O. O. Kurakevych, and T. A. Strobel, Synthesis of an open-framework allotrope of silicon, *Nat. Mater* **14**, 169 (2014).
- [9] H. I. T. Hauge, M. A. Verheijen, S. Conesa-Boj, T. Etzelstorfer, M. Watzinger, D. Kriegner, I. Zardo, C. Fasolato, F. Capitani, and P. Postorino, Hexagonal silicon realized, *Nano Lett.* **15**, 5855 (2015).
- [10] J. Tang, J.-L. Maurice, F. Fossard, I. Florea, W. Chen, E. V. Johnson, M. Foldyna, L. Yu, and P. Roca i Cabarrocas, Natural occurrence of the diamond hexagonal structure in silicon nanowires grown by a plasma-assisted vapour–liquid–solid method, *Nanoscale* **9**, 8113 (2017).
- [11] Y. Ren, P. Leubner, M. A. Verheijen, J. E. M. Haverkort, and E. P. A. M. Bakkers, Hexagonal silicon grown from higher order silanes, *Nanotechnology* **30**, 295602 (2019).
- [12] S. Pandolfi, C. Renero-Lecuna, Y. Le Godec, B. Baptiste, N. Menguy, M. Lazzeri, C. Gervais, K. Spektor, W. A. Crichton, and O. O. Kurakevych, Nature of hexagonal silicon forming via high-pressure synthesis: Nanostructured hexagonal 4H polytype, *Nano Lett.* **18**, 5989 (2018).
- [13] Z. He, J.-L. Maurice, Q. Li, and D. Pribat, Direct evidence of 2H hexagonal Si in Si nanowires, *Nanoscale* **11**, 4846 (2019).
- [14] H. M. Jennings and M. H. Richman, A hexagonal (wurtzite) form of silicon, *Science* **193**, 1242 (1976).
- [15] J. Bandet, B. Despax, and M. Caumont, Vibrational and electronic properties of stabilized wurtzite-like silicon, *J. Phys. D: Appl. Phys.* **35**, 234 (2002).
- [16] F. Fabbri, E. Rotunno, L. Lazzarini, D. Cavalcoli, A. Castaldini, N. Fukata, K. Sato, G. Salviati, and A. Cavallini, Preparing the way for doping wurtzite silicon nanowires while retaining the phase, *Nano Lett.* **13**, 5900 (2013).
- [17] C. Raffy, J. Furthmüller, and F. Bechstedt, Properties of hexagonal polytypes of group-IV elements from first-principles calculations, *Phys. Rev. B* **66**, 075201 (2002).
- [18] C. Rödl, J. Furthmüller, J. R. Suckert, V. Armuzza, F. Bechstedt, and S. Botti, Accurate electronic and optical properties of hexagonal germanium for optoelectronic applications, *Phys. Rev. Materials* **3**, 034602 (2019).
- [19] E. M. T. Fadaly, A. Dijkstra, J. R. Suckert, D. Ziss, M. A. J. van Tilburg, C. Mao, Y. Ren, V. T. van Lange, K. Korzun, S. Kölling *et al.*, Direct-bandgap emission from hexagonal ge and sige alloys, *Nature (London)* **580**, 205 (2020).
- [20] K. Sueoka, E. Kamiyama, P. Śpiewak, and J. Vanhellefont, Review—Properties of intrinsic point defects in Si and Ge assessed by density functional theory, *ECS J. Solid State Sci. Technol.* **5**, P3176 (2016).
- [21] L. Sun, M. A. L. Marques, and S. Botti, Direct insight into the structure-property relation of interfaces from constrained crystal structure prediction, *Nat. Commun.* **12**, 811 (2021).
- [22] S. Goedecker, T. Deutsch, and L. Billard, A Fourfold Coordinated Point Defect in Silicon, *Phys. Rev. Lett.* **88**, 235501 (2002).
- [23] A. R. Oganov (ed.), *Modern Methods of Crystal Structure Prediction* (Wiley-VCH Verlag GmbH & Co. KGaA, Berlin, Germany, 2010).

- [24] J. Shi, W. Cui, J. Hao, M. Xu, X. Wang, and Y. Li, Formation of ammonia–helium compounds at high pressure, *Nat. Commun.* **11**, 3164 (2020).
- [25] J. Shi, W. Cui, S. Botti, and M. A. L. Marques, Nitrogen-hydrogen-oxygen ternary phase diagram: New phases at high pressure from structural prediction, *Phys. Rev. Materials* **2**, 023604 (2018).
- [26] H. Liu, I. Naumov, R. Hoffmann, N. Ashcroft, and R. Hemley, Potential high-Tc superconducting lanthanum and yttrium hydrides at high pressure, *Proc. Natl. Acad. Sci. USA* **114**, 6990 (2017).
- [27] H. Dong, A. R. Oganov, V. V. Brazhkin, Q. Wang, J. Zhang, M. M. Davari Esfahani, X.-F. Zhou, F. Wu, and Q. Zhu, Boron oxides under pressure: Prediction of the hardest oxides, *Phys. Rev. B* **98**, 174109 (2018).
- [28] A. R. Oganov, J. Chen, C. Gatti, Y. Ma, Y. Ma, C. W. Glass, Z. Liu, T. Yu, O. O. Kurakevych, and V. L. Solozhenko, Ionic high-pressure form of elemental boron, *Nature (London)* **457**, 863 (2009).
- [29] P. Borlido, C. Steigemann, N. N. Lathiotakis, M. A. L. Marques, and S. Botti, Structural prediction of two-dimensional materials under strain, *2D Mater.* **4**, 045009 (2017).
- [30] P. Borlido, C. Rödl, M. A. L. Marques, and S. Botti, The ground state of two-dimensional silicon, *2D Mater.* **5**, 035010 (2018).
- [31] T. Gu, W. Luo, and H. Xiang, Prediction of two-dimensional materials by the global optimization approach, *WIREs Comput. Mol. Sci* **7**, e2195 (2016).
- [32] Y. Wang, M. Miao, J. Lv, L. Zhu, K. Yin, H. Liu, and Y. Ma, An effective structure prediction method for layered materials based on 2d particle swarm optimization algorithm, *J. Chem. Phys.* **137**, 224108 (2012).
- [33] Q. Zhu, A. Samanta, B. Li, R. E. Rudd, and T. Frolov, Predicting phase behavior of grain boundaries with evolutionary search and machine learning, *Nat. Commun.* **9**, 467 (2018).
- [34] Z.-L. Li, Z.-M. Li, H.-Y. Cao, J.-H. Yang, Q. Shu, Y.-Y. Zhang, H. J. Xiang, and X. G. Gong, What are grain boundary structures in graphene? *Nanoscale* **6**, 4309 (2014).
- [35] A. L.-S. Chua, N. A. Benedek, L. Chen, M. W. Finnis, and A. P. Sutton, A genetic algorithm for predicting the structures of interfaces in multicomponent systems, *Nat. Mater.* **9**, 418 (2010).
- [36] S. Botti, M. Amsler, J. A. Flores-Livas, P. Ceria, S. Goedecker, and M. A. L. Marques, Carbon structures and defect planes in diamond at high pressure, *Phys. Rev. B* **88**, 014102 (2013).
- [37] S. Goedecker, Minima hopping: An efficient search method for the global minimum of the potential energy surface of complex molecular systems, *J. Chem. Phys.* **120**, 9911 (2004).
- [38] M. Amsler and S. Goedecker, Crystal structure prediction using the minima hopping method, *J. Chem. Phys.* **133**, 224104 (2010).
- [39] S. Faraji, S. A. Ghasemi, B. Parsaeifard, and S. Goedecker, Surface reconstructions and premelting of the (100) CaF₂ surface, *Phys. Chem. Chem. Phys.* **21**, 16270 (2019).
- [40] M. Amsler, S. Botti, M. A. L. Marques, and S. Goedecker, Conducting Boron Sheets Formed by the Reconstruction of the α -Boron (111) Surface, *Phys. Rev. Lett.* **111**, 136101 (2013).
- [41] P. Borlido, A. W. Huran, M. A. L. Marques, and S. Botti, Novel two-dimensional silicon–carbon binaries by crystal structure prediction, *Phys. Chem. Chem. Phys.* **22**, 8442 (2020).
- [42] S. E. Schönborn, S. Goedecker, S. Roy, and A. R. Oganov, The performance of minima hopping and evolutionary algorithms for cluster structure prediction, *J. Chem. Phys.* **130**, 144108 (2009).
- [43] T. S. Bush, C. R. A. Catlow, and P. D. Battle, Evolutionary programming techniques for predicting inorganic crystal structures, *J. Mater. Chem.* **5**, 1269 (1995).
- [44] S. M. Woodley and R. Catlow, Crystal structure prediction from first principles, *Nat. Mater.* **7**, 937 (2008).
- [45] Y. Wang, J. Lv, L. Zhu, and Y. Ma, Crystal structure prediction via particle-swarm optimization, *Phys. Rev. B* **82**, 094116 (2010).
- [46] Y. Wang, J. Lv, L. Zhu, and Y. Ma, CALYPSO: A method for crystal structure prediction, *Comput. Phys. Commun.* **183**, 2063 (2012).
- [47] C. M. Freeman and C. R. A. Catlow, Structure predictions in inorganic solids, *J. Chem. Soc., Chem. Commun.*, 89 (1992).
- [48] B. P. van Eijck and J. Kroon, Structure predictions allowing more than one molecule in the asymmetric unit, *Acta Crystallogr. B* **56**, 535 (2000).
- [49] C. J. Pickard and R. J. Needs, High-Pressure Phases of Silane, *Phys. Rev. Lett.* **97**, 045504 (2006).
- [50] C. J. Pickard and R. J. Needs, Ab initio random structure searching, *J. Phys.: Condens. Matter* **23**, 053201 (2011).
- [51] S. S. Kapur, M. Prasad, J. C. Crocker, and T. Sinno, Role of configurational entropy in the thermodynamics of clusters of point defects in crystalline solids, *Phys. Rev. B* **72**, 014119 (2005).
- [52] S. S. Kapur and T. Sinno, Entropic origins of stability in silicon interstitial clusters, *Appl. Phys. Lett.* **93**, 221911 (2008).
- [53] P. Hohenberg and W. Kohn, Inhomogeneous electron gas, *Phys. Rev.* **136**, B864 (1964).
- [54] W. Kohn and L. J. Sham, Self-consistent equations including exchange and correlation effects, *Phys. Rev.* **140**, A1133 (1965).
- [55] S. A. Ghasemi, M. Amsler, R. G. Hennig, S. Roy, S. Goedecker, T. J. Lenosky, C. J. Umrigar, L. Genovese, T. Morishita, and K. Nishio, Energy landscape of silicon systems and its description by force fields, tight binding schemes, density functional methods, and quantum Monte Carlo methods, *Phys. Rev. B* **81**, 214107 (2010).
- [56] A. P. Bartók, J. Kermode, N. Bernstein, and G. Csányi, Machine Learning a General-Purpose Interatomic Potential for Silicon, *Phys. Rev. X* **8**, 041048 (2018).
- [57] M. R. G. Marques, J. Wolff, C. Steigemann, and M. A. L. Marques, Neural network force fields for simple metals and semiconductors: Construction and application to the calculation of phonons and melting temperatures, *Phys. Chem. Chem. Phys.* **21**, 6506 (2019).
- [58] B. Aradi, B. Hourahine, and Th. Frauenheim, DFTB+, a sparse matrix-based implementation of the DFTB method, *J. Phys. Chem. A* **111**, 5678 (2007).
- [59] A. W. Huran, C. Steigemann, T. Frauenheim, B. Aradi, and M. A. L. Marques, Efficient automatized density-functional tight-binding parametrizations: Application to group IV elements, *J. Chem. Theory Comput.* **14**, 2947 (2018).
- [60] G. Kresse and J. Furthmüller, Efficient iterative schemes for ab initio total-energy calculations using a plane-wave basis set, *Phys. Rev. B* **54**, 11169 (1996).

- [61] G. Kresse and J. Furthmüller, Efficiency of ab-initio total energy calculations for metals and semiconductors using a plane-wave basis set, *Comput. Mater. Sci.* **6**, 15 (1996).
- [62] J. P. Perdew, K. Burke, and M. Ernzerhof, Generalized Gradient Approximation Made Simple, *Phys. Rev. Lett.* **77**, 3865 (1996).
- [63] A. D. Becke and E. R. Johnson, A simple effective potential for exchange, *J. Chem. Phys.* **124**, 221101 (2006).
- [64] F. Tran and P. Blaha, Accurate Band Gaps of Semiconductors and Insulators with a Semilocal Exchange-Correlation Potential, *Phys. Rev. Lett.* **102**, 226401 (2009).
- [65] P. Borlido, T. Aull, A. W. Huran, F. Tran, M. A. L. Marques, and S. Botti, Large-scale benchmark of exchange–correlation functionals for the determination of electronic band gaps of solids, *J. Chem. Theory Comput.* **15**, 5069 (2019).
- [66] J. Heyd, G. E. Scuseria, and M. Ernzerhof, Hybrid functionals based on a screened Coulomb potential, *J. Chem. Phys.* **118**, 8207 (2003); **124**, 219906(E) (2006).
- [67] J. R. Suckert, C. Rödl, J. Furthmüller, F. Bechstedt, and S. Botti, Efficient strain-induced light emission in lonsdaleite germanium, *Phys. Rev. Materials* **5**, 024602 (2021).
- [68] M. Boujnah, H. Ennaceri, A. El Kenz, A. Benyoussef, E. Chavira, M. Loulidi, and H. Ez-Zahraouy, The impact of point defects on the optical and electrical properties of cubic ZrO₂, *J. Comput. Electron.* **19**, 940 (2020).
- [69] A. H. Reshak and S. Auluck, Influence of an oxygen vacancy on the electronic structure of the asymmetric mixed borate–carbonate Pb₇O(OH)₃(CO₃)₃(BO₃), *RSC Adv.* **6**, 18965 (2016).
- [70] X. Liu, L. Xi, W. Qiu, J. Yang, T. Zhu, X. Zhao, and W. Zhang, Significant roles of intrinsic point defects in Mg₂X (X = Si, Ge, Sn) thermoelectric materials, *Adv. Electron. Mater.* **2**, 1500284 (2016).
- [71] J. Dabrowski and G. Kissinger, Supercell-size convergence of formation energies and gap levels of vacancy complexes in crystalline silicon in density functional theory calculations, *Phys. Rev. B* **92**, 144104 (2015).
- [72] J. Zhu, Ab initio pseudopotential calculations of dopant diffusion in Si, *Comput. Mater. Sci.* **12**, 309 (1998).
- [73] A. E. Mattsson, R. R. Wixom, and R. Armiento, Electronic surface error in the Si interstitial formation energy, *Phys. Rev. B* **77**, 155211 (2008).
- [74] A. J. Morris, C. J. Pickard, and R. J. Needs, Hydrogen/silicon complexes in silicon from computational searches, *Phys. Rev. B* **78**, 184102 (2008).
- [75] See Supplemental Material at <http://link.aps.org/supplemental/10.1103/PhysRevMaterials.5.064605> for the images of the geometries of all defects with formation energies ranging from 2.52 to 7.00 eV and the corresponding cif files.
- [76] T. Kobayashi, K. Harada, Y. Kumagai, F. Oba, and Y.-i. Matsushita, Native point defects and carbon clusters in 4H-SiC: A hybrid functional study, *J. Appl. Phys.* **125**, 125701 (2019).
- [77] J. Xi, B. Liu, Y. Zhang, and W. J. Weber, Ab initio study of point defects near stacking faults in 3C-SiC, *Comput. Mater. Sci.* **123**, 131 (2016).
- [78] M. G. Ganchenkova, I. A. Supryadkina, K. K. Abgaryan, D. I. Bazhanov, I. V. Mutigullin, and V. A. Borodin, Influence of the ab-initio calculation parameters on prediction of energy of point defects in silicon, *Mod. Electron. Mater.* **1**, 103 (2015).
- [79] M. Posselt, F. Gao, and D. Zwicker, Atomistic study of the migration of di- and tri-interstitials in silicon, *Phys. Rev. B* **71**, 245202 (2005).
- [80] O. K. Al-Mushadani and R. J. Needs, Free-energy calculations of intrinsic point defects in silicon, *Phys. Rev. B* **68**, 235205 (2003).
- [81] Sholihun, M. Saito, T. Ohno, and T. Yamasaki, Density-functional-theory-based calculations of formation energy and concentration of the silicon monovacancy, *Jpn. J. Appl. Phys.* **54**, 041301 (2015).
- [82] P. Seeberger and J. Vidal, On the *ab initio* calculation of vibrational formation entropy of point defect: The case of the silicon vacancy, *EPJ Photovolt.* **8**, 85505 (2017).